Model-based controller design for antagonistic pairs of fluidic muscles in manipulator motion control

Frank Schreiber, Yevgen Sklyarenko, Gundula Runge, Marcus Grobe and Walter Schumacher

***Abstract*— A control structure is presented for manipulators actuated by joints with pairwise antagonistic pneumatic muscles. The used muscles and the resulting behavior of a single manipulator joint featuring antagonistic muscles in a symmetric configuration are characterized.**

Pneumatic joint actuation results in a hysteretic behavior, it is shown that in this case the hysteresis can be described by a Preisach hysteresis model. This hysteresis model allows the construction of a model-reference following controller with a model control loop designed for good tracking performance and a disturbance rejection loop optimized for suppression of disturbances.

Experiments confirm the improvement in tracking control as compared to the system solely controlled by a feedback regulator.

I. Introduction

Pneumatic muscles have matured to become reliable, highly durable low cost actuators. Due to favorable characteristics such as high power-to-weight ratio and their inherent compliance, they are well-suited for the design of lightweight versatile robots [1], [2].

A. Muscle characteristics

Most of the pneumatic muscles in use today are based on the McKibben artificial muscle, consisting of an air proof so-called rubber bladder which is surrounded by a sheath of inextensible fibers and closed at both ends by caps [3]. When pressurized, the bladder increases in volume, resulting in an expansion in radius and an axial contraction due to the inextensible sheath. When attached to an appropriate bearing, the pressurized muscle is able to exert a pulling force. When the pressure is released, the deformed muscle relaxes slowly, allowing it to passively return to its original shape. When expanding against an opposing force the muscle is prone to buckling. Therefore, just like their natural counterparts, pneumatic muscles can only feasibly exert pulling forces and have to be used in an antagonistic setup. One of the main challenges in the application of artificial pneumatic actuators is their difficult controllability, as the available muscles exhibit a wide range of nonlinear effects. Apart from omnipresent creep, their deflection, which can reach values of up to 25% of the muscle length in the unloaded case, is dependent upon the applied air pressure and the acting force. Due to frictional effects in the air path and the muscle material, the deflection exhibits an asymmetrically hysteretic behavior, see filled areas in Figure 1, which prohibits the precise open loop control of a single muscle. The manufacturer guarantees a contraction hysteresis of at most 3% of the nominal length. The deflection error of the muscle due to the hysteresis can thus reach values of over 10% of the possible stroke.

All authors are with the Institute of Control Engineering, Technische Universität Braunschweig, 38106 Braunschweig, Germany.

Corresponding author: schreiber@ifr.ing.tu-bs.de

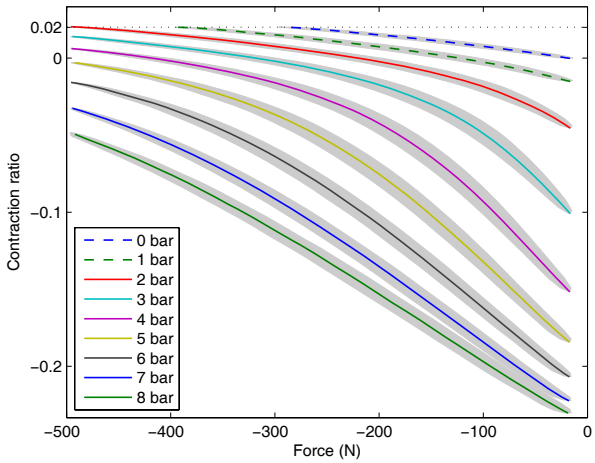

Fig. 1. Hysteretic behavior of the isobarically loaded muscle. Contraction forces and displacements are denoted with a negative sign.

The gray contours in Figure 1 depict the load force and contraction loops measured at different air pressures at a frequency of 0.1 Hz, acquired for a pneumatic muscle of type DMSP-10-150N manufactured by FESTO. To derive a description for the mean relation between contraction and load force for a given air pressure, the mean force for a certain length is calculated from the flanks of the loops and displayed as a colored line. The resulting mapping is given in Figure 2.

An abundance of approaches has been suggested to model the resulting mapping [4], [5], [6]. Boblan et al. compare several possible approaches to describe the static relation between contraction, pressure and muscle force [7]. He concludes that the static relation of a single muscle can be described with best accuracy by a sine model, consisting of a superposition of linear and sinusoid components. Therefore, a sine model approach was chosen in our investigations and parameterized using the measured data displayed in Figure 2. Consequently, this model was inverted to provide the necessary air pressure for an admissible combination of muscle contraction and muscle force.

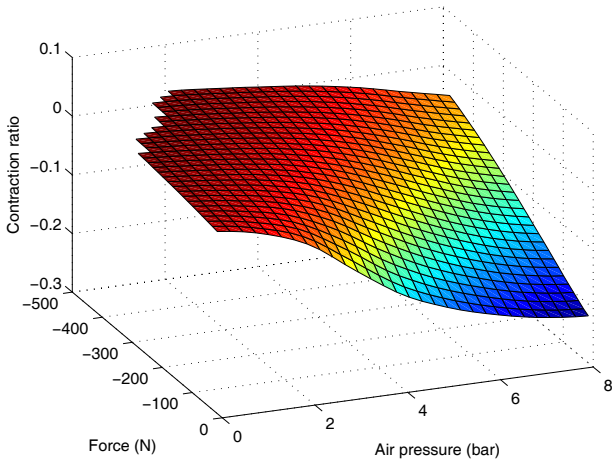

Fig. 2. Static characteristics of used muscle type.

B. Manipulator setup

Fig. 3 (left) depicts the manipulator structure as introduced by Schmitt et al. in [1]. A single stage consists of a pair of antagonistic pneumatic muscles manufactured by FESTO of type DMSP-10-150N, possessing a working length of 150 mm and a muscle diameter of 10 mm. From the module design depicted in Fig. 3 (right), the relation between the joint angle φ and the corresponding effective actuator lengths L_A and L_B can be derived:

$$\begin{aligned} L_A &= \left| \begin{pmatrix} r_u \\ l_u \end{pmatrix} + \begin{pmatrix} cos\varphi & -sin\varphi \\ sin\varphi & cos\varphi \end{pmatrix} \cdot \begin{pmatrix} -r_o \\ l_o \end{pmatrix} \right|, \\ L_B &= \left| \begin{pmatrix} -r_u \\ l_u \end{pmatrix} + \begin{pmatrix} cos\varphi & -sin\varphi \\ sin\varphi & cos\varphi \end{pmatrix} \cdot \begin{pmatrix} r_o \\ l_o \end{pmatrix} \right|. \end{aligned} \quad (1)$$

An inverse mapping of the muscle statics is derived by combining the kinematics of a single segment in (1) and the static mapping relating the air pressure and the applied force to the resulting mean contraction in Fig. 2. This inverse mapping provides the necessary air pressures in each muscle for a combination of desired joint angle and individual muscle forces and is integrated in a feedforward control structure as displayed in Fig. 4. The described feedforward structure compensates the static nonlinear relations between the mean values of the contraction force and displacement to the pressure. Depending on the combination of the muscle forces, drive torques as well as antagonistic torques will be produced. The antagonistic torques do not result in any motion, as they merely cause a prestress in both actuators, that can be used to vary the joint's stiffness [8]. In the following, the external force input is only used to generate a prestress in the system.

In the antagonistic setup the same effects causing hysteretic behavior in a single muscle will result in a hysteretic behavior between the desired and the measured joint angle due to the symmetric setup of the joint actuators the resulting hysteretic behavior will consequently be symmetric.

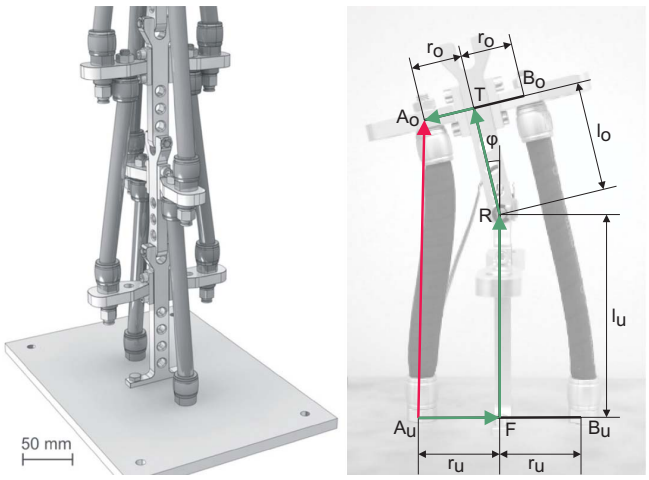

Fig. 3. Manipulator structure (left) and kinematic setup of a single manipulator segment (right).

II. Preisach hysteresis model of the antagonistically actuated segment

A variety of hysteresis models have been applied in an attempt to model the inherent hysteretic behavior of pneumatic muscle actuators. Minh et al. successfully demonstrated the application of a Maxwell-slip-model for the description of the contraction length to force behavior for a single muscle [9], as well as for the torque hysteresis for the movement in a joint driven by an antagonistic muscle pair [10]. Schindele presented the modeling of the force-volume-characteristics based upon a Bouc-Wen-Model [**?**]. While the described modeling results provide a good reproduction of the behavior of single muscles, no control approach is presented that can be extended to incorporate the control of a joint driven by an antagonistic muscle pair. Attempts have been made to apply classic hysteresis modeling approaches such as Preisach models to the modeling and control of pneumatic muscles and pairs of pneumatic muscles [12], [13].

The results obtained in these works provided only limited, superficial modeling success. The congruency condition, which is an important necessary precondition to ensure the applicability of a Preisach-approach [14], is not fulfilled by the asymmetric hysteretic behavior of a single pneumatic

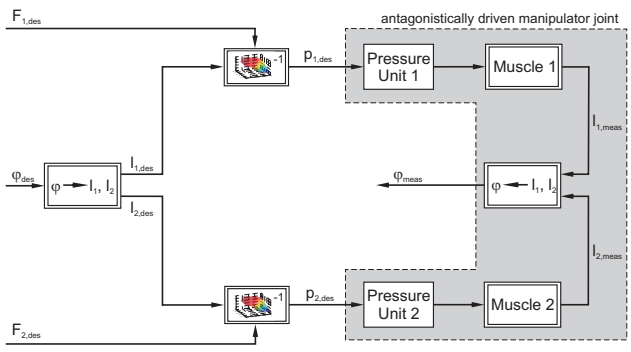

Fig. 4. feedforward joint angle control.

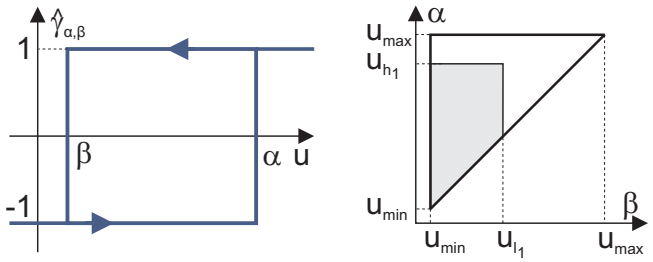

Fig. 5. An elementary hysteresis operator $\hat{\gamma}$ (left) and Preisach plane (right).

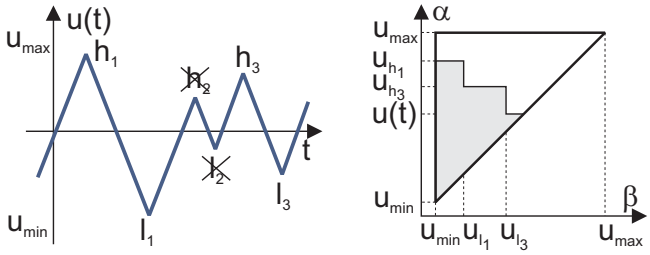

Fig. 6. Input sequence with dominant, as well as wiped out extremal values (left) and Preisach plane with correspondingly activated elemental operators (right).

muscle. Therefore the models derived in these works were only able to reproduce major loops similar to ones used in the identification process of the model. The main potential of a Preisach model, the ability to model the minor loop behavior and the model inversion for an approximate compensation of the hysteresis could therefore not be exploited. It will be shown that the use of the presented symmetrical antagonistic setup featuring a pneumatic muscle pair with a compensation of the static mean nonlinear force-contraction-pressure characteristics results in a symmetrical hysteresis behavior which fulfills all necessary conditions to allow modeling by a Preisach model.

A. *Preisach model of hysteresis*

The Preisach hysteresis model was first developed by Preisach in 1935 in an attempt to model the physical mechanisms of magnetization [15]. Although it was first regarded to be a physical model of hysteresis, the Preisach model turned out to be a phenomenological model that has mathematical generality and is applicable to phenomena from many disciplines. A rigid mathematical generalization has been presented by Mayergoyz, who also determined the necessary conditions for the applicability of such a model [16].

The simplest type of hysteresis operator $\hat{\gamma}_{\alpha\beta}$ can be represented as rectangular loops in the in-/output-plane, as shown in Fig. 5 (left). Its output switches between $+1$ and -1 depending on the initial output and the history of past inputs, representing a local memory. In addition to the set of operators $\hat{\gamma}_{\alpha\beta}$, with α and β corresponding to the "up" and "down" switching values of the input $u(t)$, a weighting function $\mu(\alpha, \beta)$ must be considered, which is called the Preisach function and can be identified for a given system. The resulting Preisach model with the system output $f(t)$ is then given by

$$f(t) = \int\int_{\alpha \geq \beta} \mu(\alpha, \beta) \hat{\gamma}_{\alpha\beta}\left(u(t)\right) d\alpha d\beta. \tag{2}$$

The switching values are subject to the relation $u_{max} \geq \alpha \geq \beta \geq u_{min}$, with u_{max} and u_{min} being determined by the system's physical properties. The feasible combinations of α and β for the triangle T are displayed in Fig. 5 (right). The output of the Preisach model is determined by integrating the product of the weighting function $\mu(\alpha, \beta)$ and the operator $\hat{\gamma}_{\alpha\beta}$ over the triangle T. The model output is dependent on the extremal values in the history of the input sequence $u(t)$ as depicted in the example in Fig. 6. The set of dominant maxima and minima determines the output of the system, due to the wipe-out property of the Preisach model, input values larger than past dominant maxima or smaller than past minima wipe out the effects of the older extrema. The dominant extrema are marked in the input sequence depicted in Fig. 6 (left). At any instant the Preisach plane can be divided into two regions, the one in which the relay operator outputs are $+1$, marked dark gray in Fig. 6 (right), and the one in which the relays' outputs are -1. Both areas are separated by a descending staircase function, whose corners are determined by the past reversal points in the input sequence. After applying the identification algorithm presented by Mayergoyz to determine the Preisach function from first order descending curves [14], the Everett map E is defined [17], which contains the change of the output value $f(t)$ as a function of α and β:

$$E(u_\alpha, u_\beta) = f_\alpha - f_{\alpha\beta}. \tag{3}$$

Since $\alpha \geq \beta$ during the measurement, only one half of the map can be constructed by measurements. The missing values are given by $f_{\alpha\beta} = -f_{\beta\alpha}$. Thus the value of $f_{\alpha\beta}$ can be calculated for any single combination of α and β. With the sets of past dominant maxima H and dominant minima L, the Preisach model output can then be expressed for any given sequence of inputs $u(t)$ by

$$\begin{aligned} f(t) \;=\; & f_{min} + \sum_{k=1}^{n(t)-1} \left[f_{H_k,L_k} - f_{H_k,L_{k-1}}\right] \ldots \\ & + \begin{cases} \left[f_{H_n,u(t)} - f_{H_n,L_{n-1}}\right] & \text{if } \dot{u}(t) \leq 0, \\ \left[f_{u(t),u(t)} - f_{u(t),L_{n-1}}\right] & \text{if } \dot{u}(t) \geq 0, \end{cases} \end{aligned} \tag{4}$$

with f_{min} being the output corresponding to $u = u_{min}$ (all relays set to -1).

For a given Preisach model a computationally compact inverse can be derived from (5) if the first-order curve data surfaces $f_{\alpha\beta}$ are strictly monotonically increasing with respect to the parameters α and β. This will result in the inverse of the Everett map G, given by

$$G(f_\alpha, f_{\alpha\beta}) = u_\alpha - u_\beta. \tag{5}$$

With this mapping the unknown input $u(f(t))$ to achieve the

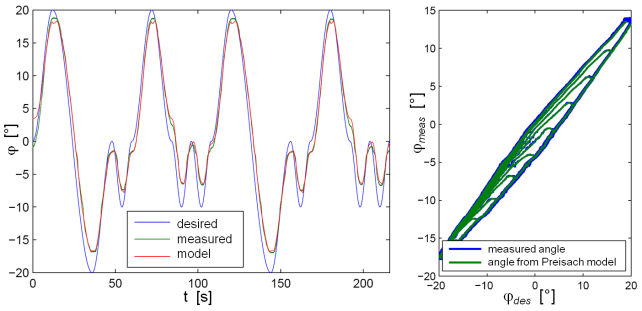

Fig. 7. Comparison of hysteretic behavior model and measurements.

desired output $f(t)$ can be computed using

$$u(f(t)) = u_{min} + \sum_{i=1}^{k-1} G\left(F_{d_{i+1}}, F_{d_i}\right) + G\left(f(t), F_{d_k}\right), \quad (6)$$

with F_d being the set of past output extreme values.

Mayergoyz recognized that a hysteresis nonlinearity can only be represented by a Preisach model if it fulfills the wiping-out property and minor-loop congruence property conditions [16]. The fulfillment of the properties by the used system was shown in [18].

B. Identification and feedforward compensation

The hysteretic behavior of the system was identified by producing a series of first order descending curves. An input signal was chosen to lead the output along an ascending branch of the major loop. At distinct values, chosen as suggested in [19], the input slope is reversed producing a descending curve in the input-output-diagram that terminates at negative saturation. Due to the symmetric hysteresis loop it is apparent, that the relation

$$\mu(\alpha, \beta) = \mu(-\beta, -\alpha) \quad (7)$$

is valid. Therefore it is obvious, that for the identification of $\mu(\alpha, \beta)$ also the first-order increasing curves could have been used which are attached to the limiting descending branch.

After the derivation of the inverse Preisach model, as presented in [20], the desired joint angle is fed into the inverse model whose output serves as the input to the feedforward structure in Fig. 4.

C. Comparison of hysteresis model and plant behavior

Figure 7 shows a comparison of the modeled and the measured hysteretic plant behavior for quasistatic movements. It can be shown that the static hysteresis nonlinearity is reproduced by the derived Preisach hysteresis model. Minor deviations occur in the vicinity of turning points which decay along the further movement.

III. Controller design

To ensure precise tracking in the presence of disturbances, creep, and model uncertainties, it is imperative to complement the feedforward compensator with a feedback controller. The idea of the control scheme, depicted in Fig. 8, is to combine the feedforward hysteresis compensator and a model-following controller (MFC) based on the nominal dynamic model to implement an effective tracking controller. The fundamental idea behind the model-following controller structure is to separate the tracking control from the disturbance rejection problem in the controller design, by including a plant model in the model control loop which is controlled by the tracking controller. As the model control loop is disturbance free, the tracking controller can thus be designed to provide good tracking performance. The output of the plant model serves as reference value to the disturbance rejection loop containing the actual plant, providing a filtered reference. The main advantage of the setup is that the inverse plant model, which is usually needed for feedforward control, does not need to be calculated, as all the signals in the control loop can be calculated with the direct model.

The controller output in the model loop, which is necessary to produce an output of φ_{mod} is known. The output of the tracking controller provides a feedforward control signal which compensates the dynamic behavior modeled in the previous loop and is added to the output of the disturbance rejection controller. If the plant model reflects the exact behavior of the actual plant, the plant will be driven to the desired values by the feedforward signal alone. As there are always modeling errors and disturbances acting on the actual plant, the disturbance rejection controller has to compensate those effects. Since the controller in the model loop provides for the tracking performance, the controller of the second loop with the actual plant can be designed solely for good disturbance rejection. Since there is only a feedforward connection between the loops, the stability of the control system is not compromised, as long as the stability of the individual control loops is ensured. For more information regarding MFC see Osypiuk et al. in [21]. Due to the hysteretic behavior of the plant, its gain is dependent upon the current amplitude and direction, while it shows a similar dynamic behavior over the range of possible joint angles. A typical step response along with an approximation of the dynamic behavior as a second order system with two real poles at $s = 23rad/s$ is shown in Fig. 9. The gain of the nominal plant model is derived from the in-/output characteristic as shown in Fig. 9. With this model a PI controller is designed such that one of the poles is canceled, while the gain is set to provide for a damping of $D = 1/\sqrt{2}$.

The hysteresis nonlinearity induces an uncertainty in the gain parameter of the plant which has to be taken into account in the controller design for the disturbance rejection loop. Although the resulting hysteretic loops lead to a parametric uncertainty, the maximal and minimal possible gain values can be derived from the in-/output hysteretic characteristic of the plant. On any point of a minor loop, the slope of the tangent can be regarded as the instantaneous gain. The extremal gains on a minor loop define the range of gain uncertainty along this minor loop, which can be seen as the bounding sector indicated in Fig. 10. As shown in Sec. II-C the hysteretic plant's in-/output behavior can be described by the derived Preisach model. The minor loops can therefore be described by the measured Everett maps, see

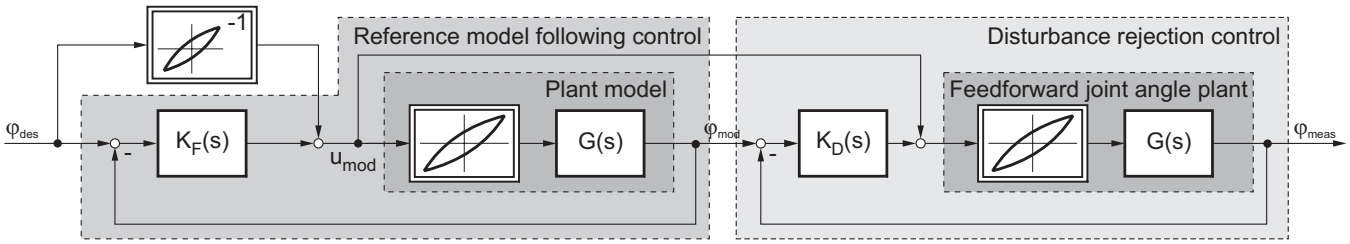

Fig. 8. Control structure with feedforward hysteresis compensator and model-following controller consisting of model and disturbance rejection loop.

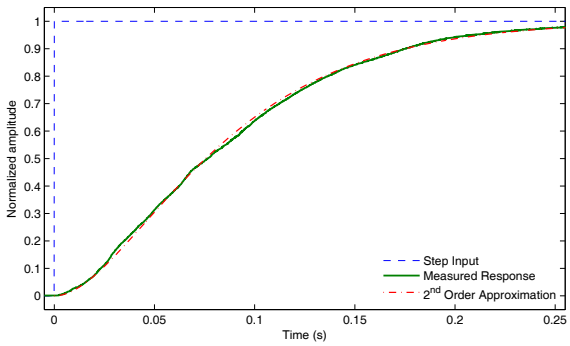

Fig. 9. Normalized step response of the joint angle plant, as mean of rising and falling step.

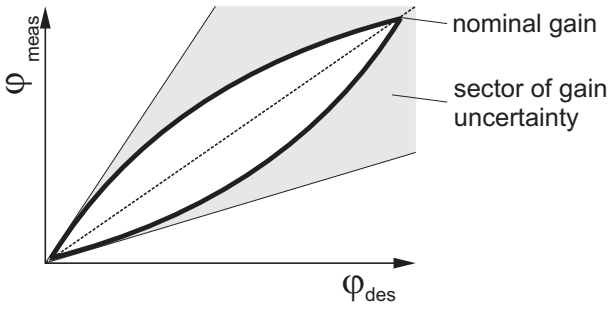

Fig. 10. Schematic of the gain approximation from the hysteretic characteristics.

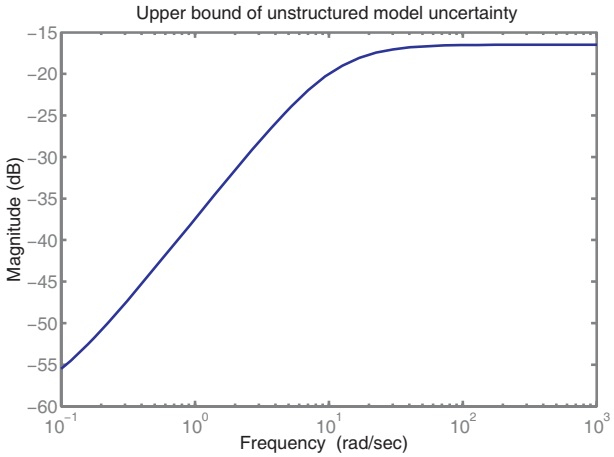

Fig. 11. Selected function bounding the considered unstructured uncertainties.

Fig.7 (right). The gain in any points along minor loops then corresponds to the derivative of the Everett map $E(u_\alpha, u_\beta)$ for this combination of α and β. It follows that the bounds of the gain uncertainty between input and output within the major loop can then be determined by calculating the maximal and minimal slope on the Everett map.

Along with the parameter uncertainty, an unstructured uncertainty bounded by the function displayed in Fig. 11 is taken into account in the controller design process, to account for higher frequency influences and modeling errors. To ensure a good disturbance rejection, especially for stationary and low frequency disturbances acting at the plant output, the sensitivity function is weighted accordingly in the H_∞-controller design. The disturbance rejection controller is then derived as a robust controller for the uncertain open-loop plant model via the μ-synthesis, as described in [22].

Figure 12 shows a comparison of the step response behaviors of the controlled joint angle. It can be seen, that the system's tracking dynamics clearly benefits from the model-following control design. While showing comparable overshoot, the output's rise time is significantly reduced by the combination of inverse Preisach feedforward compensation in combination with the reference model following control loop. The disturbance rejection controller, which can be designed specifically for this purpose, allows a significant reduction of the influence of high frequency noise and load fluctuations resulting from stick effects in manipulator joints.

IV. Conclusion

In this paper the control architecture for a manipulator actuated by pneumatic artificial muscles is presented. After a brief description of the used muscle type and its pressure-force-length-relations, these characteristic are used to implement a feedforward structure for the control of a single pair of antagonistic muscles in the manipulator structure.

Due to the symmetric setup of the muscles in the used manipulator and the feedforward structure, the nonlinear mean relation of the muscles are compensated in the unloaded case resulting in a symmetric hysteresis of the open loop plant between desired and measured joint angle. It can be shown, that this symmetric hysteresis nonlinearity fulfills all necessary conditions to describe it by a Preisach model approach. A Preisach model is identified, its inverse is used for an approximate feedforward compensation of the hysteresis nonlinearity.

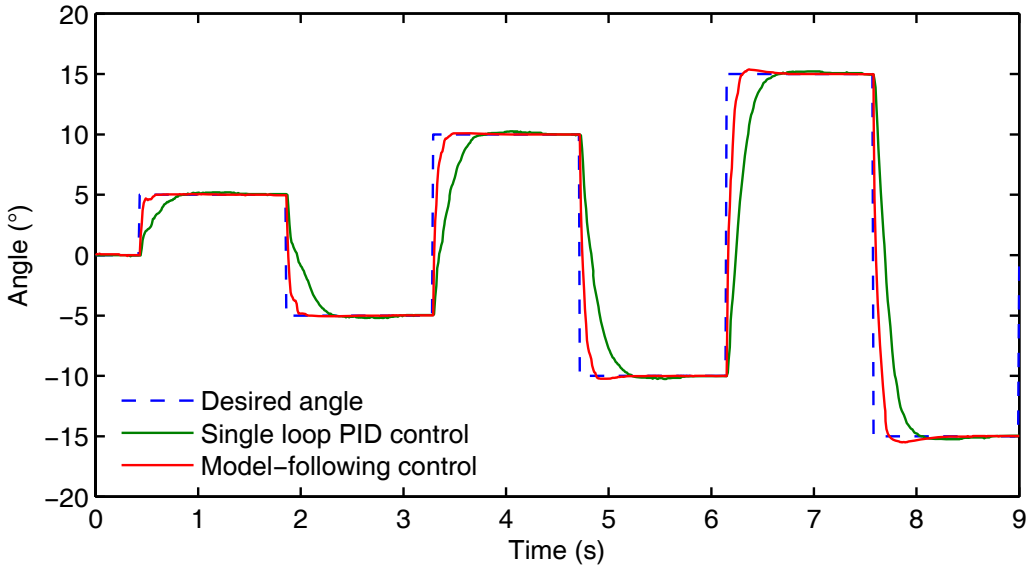

Fig. 12. Step response experiment performed with a single manipulator stage controlled by a single loop PID controller (green) and by model-following controller (red).

The joint controllers are realized as a model-following controller, the direct and inverse Hysteresis model is used to control the model-control loop, its controller output is fed into the disturbance rejection loop as a feedforward term. The controller of the model loop is designed for good tracking performance, while the disturbance rejection controller is optimized for good disturbance rejection in the presence of disturbances and parametric uncertainties. Measurements are presented to demonstrate that the resulting controller outperforms comparable single loop controllers in experimental investigation.

REFERENCES

[1] J. Schmitt, F. Grabert, and A. Raatz, "Design of a hyper-flexible assembly robot using artificial muscles," in *Robotics and Biomimetics (ROBIO), 2010 IEEE International Conference on*, dec. 2010, pp. 897 –902.

[2] I. Boblan, R. Bannasch, A. Schulz, and H. Schwenk, "A human-like robot torso ZAR5 with fluidic muscles: Toward a common platform for embodied AI," in *50 Years of Artificial Intelligence*, ser. Lecture Notes in Computer Science, M. Lungarella, F. Iida, J. Bongard, and R. Pfeifer, Eds. Springer Berlin / Heidelberg, 2007, vol. 4850, pp. 347–357.

[3] F. Daerden and D. Lefeber, "Pneumatic artificial muscles: Actuators for robotics and automation," *European Journal of Mechanical and Environmental Engineering*, vol. 47, pp. 10–21, 2000.

[4] D. Schindele and H. Aschemann, "Disturbance compensation strategies for a high-speed linear axis driven by pneumatic muscles," in *Proceedings of the European Control Conference 2009*, August 2009, pp. 436–441.

[5] C.-P. Chou and B. Hannaford, "Measurement and modeling of McKibben pneumatic artificial muscles," *IEEE Transactions on Robotics and Automation*, vol. 12, no. 1, pp. 90–102, Feb. 1996.

[6] S. S. Mena, S. Sesmat, and E. Bideaux, "Parallel Manipulator driven by Pneumatic Muscles," in *Proc. of 8th International Fluid Power Conference*, vol. 1, 2012, pp. 163–174.

[7] I. Boblan, "Modellbildung und Regelung eines fluidischen Muskelpaares," Ph.D. dissertation, Fakultät III - Prozesswissenschaften - der Technischen Universität Berlin, 30. November 2009.

[8] I. Sardellitti, G. Palli, N. Tsagarakis, and D. Caldwell, "Antagonistically actuated compliant joint: Torque and stiffness control," in *IEEE/RSJ International Conference on Intelligent Robots and Systems (IROS)*, oct. 2010, pp. 1909 –1914.

[9] T. Minh, T. Tjahjowidodo, H. Ramon, and H. Van Brussel, "A new approach to modeling hysteresis in a pneumatic artificial muscle using the maxwell-slip model," *IEEE/ASME Transactions on Mechatronics*, vol. 16, no. 1, pp. 177 –186, feb. 2011.

[10] T. Minh, B. Kamers, T. Tjahjowidodo, H. Ramon, and H. Van Brussel, "Modeling torque-angle hysteresis in a pneumatic muscle manipulator," in *IEEE/ASME International Conference on Advanced Intelligent Mechatronics (AIM)*, july 2010, pp. 1122 –1127.

[11] D. Schindele and H. Aschemann, "Modellbasierte Kompensation der Hysterese in der Kraftcharakteristik von pneumatischen Muskeln," in *46. Regelungstechnisches Kolloquium*, 2012.

[12] M. Van Damme, P. Beyl, B. Vanderborght, R. Van Ham, I. Vanderniepen, R. Versluys, F. Daerden, and D. Lefeber, "Modeling hysteresis in pleated pneumatic artificial muscles," in *IEEE Conference on Robotics, Automation and Mechatronics*, sept. 2008, pp. 471 –476.

[13] T. Kosaki and M. Sano, "Control of a parallel manipulator driven by pneumatic muscle actuators based on a hysteresis model," *Journal of Environment and Engineering*, vol. 6, no. 2, pp. 316–327, 2011.

[14] I. Mayergoyz, "Mathematical models of hysteresis," *IEEE Transactions on Magnetics*, vol. 22, no. 5, pp. 603 – 608, sep 1986.

[15] F. Preisach, "Über die magnetische Nachwirkung," *Zeitschrift fur Physik*, vol. 94, pp. 277–302, May 1935.

[16] I. D. Mayergoyz, *Mathematical Models of Hysteresis and Their Applications*, 2nd ed. Academic Press, 2003.

[17] D. H. Everett, "A general approach to hysteresis. part 4. an alternative formulation of the domain model," *Trans. Faraday Soc.*, vol. 51, pp. 1551–1557, 1955.

[18] F. Schreiber, Y. Sklyarenko, K. Schlüter, J. Schmitt, S. Rost, A. Raatz, and W. Schumacher, "Tracking control with hysteresis compensation for manipulator segments driven by pneumatic artificial muscles." in *IEEE International Conference on Robotics and Biomimetics*, 2011.

[19] F. Li and J. Zhao, "Discrete methods based on first order reversal curves to identify Preisach model of smart materials," *Chinese Journal of Aeronautics*, vol. 20, no. 2, pp. 157 – 161, 2007.

[20] D. Hughes and J. T. Wen, "Preisach modeling of piezoceramic and shape memory alloy hysteresis," *Smart Mater. Struct.*, vol. 287, no. 6, pp. 287–300, 1997.

[21] R. Osypiuk, B. Finkemeyer, and F. M. Wahl, "Multi-loop model-based control structure for robot manipulators," *Robotica*, vol. 23, no. 4, pp. 491–499, 2005.

[22] K. Zhou and J. C. Doyle, *Essentials of Robust Control*. Prentice Hall, 1999.